Biomaterials Advances 156 (2024) 213713

Contents lists available at ScienceDirect

Biomaterials Advances

journal homepage: www.journals.elsevier.com/materials-science-and-engineering-c

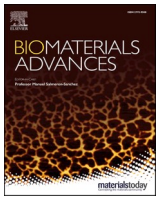

A poly(amidoamine)-based polymeric nanoparticle platform for efficient *in vivo* delivery of mRNA

Adriano P. Pontes [a], Steffen van der Wal [a], Karin Roelofs [a], Anne Grobbink [a], Laura B. Creemers [b], Johan F.J. Engbersen [a,c], Jaap Rip [a,*]

[a] 20Med Therapeutics B.V., Galileiweg 8, 2333 BD Leiden, the Netherlands
[b] Department of Orthopedics, University Medical Center Utrecht, Heidelberglaan 100, 3584 CX Utrecht, the Netherlands
[c] Technical Medical Centre, University of Twente, P.O. Box 217, 7500 AE Enschede, the Netherlands

ARTICLE INFO

Keywords:
Non-viral gene delivery
Nanoparticle
Polymer
mRNA delivery
Poly(amidoamine)

ABSTRACT

The successful use of mRNA vaccines enabled and accelerated the development of several new vaccine candidates and therapeutics based on the delivery of mRNA. In this study, we developed bioreducible poly (amidoamine)-based polymeric nanoparticles (PAA PNPs) for the delivery of mRNA with improved transfection efficiency. The polymers were functionalized with chloroquinoline (Q) moieties for improved endosomal escape and further stabilization of the mRNA-polymer construct. Moreover, these PAAQ polymers were covalently assembled around a core of multi-armed ethylenediamine (Mw 800, 2 % *w*/w) to form a pre-organized polymeric scaffolded PAAQ (ps-PAAQ) as a precursor for the formation of the mRNA-loaded nanoparticles. Transfection of mammalian cell lines with EGFP mRNA loaded into these PNPs showed a favorable effect of the Q incorporation on GFP protein expression. Additionally, these ps-PAAQ NPs were *co*-formulated with PEG-polymer coatings to shield the positive surface charge for increased stability and better *in vivo* applicability. The ps-PAAQ NPs coated with PEG-polymer displayed smaller particle size, electroneutral surface charge, and higher thermal stability. Importantly, these nanoparticles with both Q and PEG-polymer coating induced significantly higher luciferase activity in mice muscle than uncoated ps-PAAQ NPs, following intramuscular injection of PNPs loaded with luciferase mRNA. The developed technology is broadly applicable and holds promise for the development of new nucleotide-based vaccines and therapeutics in a range of infectious and chronic diseases.

1. Introduction

Efficient non-viral delivery of nucleic acids is broadly applicable in vaccines and therapeutics [1]. After the successful development of the lipid nanoparticle-based COVID-19 vaccines, there is an increased interest in mRNA delivery for different clinical applications. Encapsulation of mRNA in nanoparticles (NPs) has shown to be an effective strategy to protect the nucleic acids from degradation by extracellular exonucleases, therefore improving stability and drug efficacy [2]. Multiple strategies to encapsulate nucleic acids have been described, with the two major research areas focusing on either polymer-based system (polymeric nanoparticles – PNPs) or lipid-based systems (lipid nanoparticles – LNPs). Liposomes and LNPs were the first nanocarriers approved by the FDA and have potentially many therapeutic applications apart from the current COVID-19 mRNA-LNPs vaccines, ushering in a new era of mRNA-nanomedicine [3]. LNPs are considered to be an efficient drug delivery system due to their high translation ability, biocompatibility and low toxicity [4]. Other delivery technologies are under development, aiming for improved efficiency, (thermo)stability, lower cost of goods, easier manufacturing, and having their own IP position.

Although less advanced in the clinic than lipids, one of the most promising nanoparticular system approaches is the use of PNPs. They have potential for providing unique features, such as the assembly of nanostructures in aqueous conditions, ability of lyophilization and long-term storage, and favorable pharmacokinetics [5]. The polymer design is crucial for the efficiency of mRNA delivery. Cytotoxicity can be strongly influenced by the molecular weight of a cationic polymer and the carrier-to-RNA ratio. The addition of labile bonds such as ester or disulfide groups can improve biocompatibility and reduce toxic effects

* Corresponding author.
E-mail address: Rip@20medtx.com (J. Rip).

https://doi.org/10.1016/j.bioadv.2023.213713
Received 19 July 2023; Received in revised form 20 October 2023; Accepted 26 November 2023
Available online 30 November 2023

[6]. Endosomal escape is a major barrier towards cytosolic delivery of mRNA. The incorporation of ionizable amine groups can improve escape by changing from protonated to deprotonated states as pH decreases during endosome maturation [2]. It was shown that an apparent pKa range of 6–7 is the optimum range for the development of highly efficient nanoparticles for RNA delivery [7]. The polycation/mRNA binding can be improved by tuning polycation properties such as hydrophobicity, flexibility and hydrogen bonding, or alternatively by integrating stimuli-responsive crosslinking moieties [5]. As one of the most widely-used cationic polymers for nucleic acid delivery, polyethyleneimine (PEI) is still a benchmark for *in vitro* transfection reagents due to its low cost, relatively high efficiency and ability to release nucleotide payload outside of the endosome [8]. However, *in vivo* use is hampered by the relatively high toxicity of high molecular weight PEI and the instability of the polymer-payload complex. Biodegradable cationic polymers such as poly(amidoamine)s (PAAs) [9,10] and poly(β-amino ester) (PBAEs) [11,12] have later emerged as promising polymeric nanocarriers for gene therapy, due to their near-optimal buffering range for transfection, high efficiency and straightforward manufacture with ability to incorporate a wide variety of functional groups [13,14]. Linear PAA polymers with different (side-chain) functionalization and with different lengths were previously compared and examined for *in vitro* transfection efficiency [15–19]. The linear polymers have residual reactive groups on their termini that can be further extended with small bis-amine linkers [15]. This further enhances the efficiency of the platform by adding chemical functionality to the polymer and providing an increase in length of the linear polymers, which may improve delivery efficiency in a bioreduction-dependent manner [20].

In this paper we describe the design, synthesis, and physicochemical properties of a novel polyfunctionalized PAA that readily forms stable PNPs with mRNA and shows both *in vitro* and *in vivo* transfection results that are very promising for future application. Several bioresponsive functions are incorporated in the polymer and the PNPs made thereof. (i) As already previously described [15], the presence of tertiary amines in the main chain of the PAA polymer gives the PNPs a near-ideal buffer capacity, buffering the pH change from *ca.* 7.4 in the extracellular environment to *ca.* 5.1 in the endosomal environment. (ii) Also based on our previous studies [15,16,21–23], disulfide moieties in the main chain of the PAA chain have been included to promote the release of the nucleotide payload once the PNPs have arrived in the reductive environment of the cytosol. The presence of high concentrations of glutathione [24] in the cytosol cleaves the disulfide bonds of the polymer and consequently induces a fast degradation of the PNP carrier. (iii) Previous studies have shown that entrapment of nanoparticles in the endocytic pathway, and their resulting degradation in lysosomes, represents a major bottleneck to transfection efficiency [25,26]. Molecules or specific moieties that avoid or reduce the lysosomal degradation pathway would enable higher release of the payload into the cytosol, and could accordingly result in a significant improvement of efficacy. Since chloroquine, a small molecule containing the chloroquinoline moiety (Q), is well known as an enhancer of endosomal release in *in vitro* transfection studies [27], we have investigated the possibility to optimize mRNA delivery in eukaryotic cells by incorporating Q in the PAA polymeric system and functionalized the PAA polymers with various percentages of Q in the side chains. (iv) In the next step, the chloroquinoline-functionalized PAAQ polymer has been used to make a novel type of branched PAAQ polymer by reaction of this PAAQ with multi-armed ethylenediamine (Mw 800, 2 % *w*/w). In this manner, by covalent assembly of PAAQ polymers, a pre-organized polymeric scaffolded PAAQ is formed (ps-PAAQ). Such a scaffold is expected to enhance nucleotide binding due to reduced entropy losses during the polymer-nucleotide binding process to form loaded ps-PAAQ-based NPs and to contribute to the stability of the mRNA-loaded nanoparticle.

Although cationic NPs are easily internalized by cells *in vitro* due to their positive surface charge, the *in vivo* application may be hampered by limited biodistribution and possible side effects after administration [28,29]. In order to improve the biophysical and chemical properties of nanoparticles for *in vivo* applications, surface adsorption or grafting with shielding groups, in particular polyethylene glycol (PEG), is widely used. PEG shows remarkable hydrophilicity and electrical neutrality [30,31], while on the surface of NPs it is responsible for colloidal stability through steric repulsion, which tends to increase with the increase of the length of PEG chains [32]. Additionally, PEG prevents the nonspecific adsorption of plasma proteins and the resulting clearance by the mononuclear phagocytic system (MPS) through opsonization and activation of the complement system [33,34]. In preclinical and clinical studies with LNP-mRNA formulations, the functionalization with PEG has shown to improve nanoparticle properties, such as particle stability, delivery efficacy, tolerability and biodistribution [35]. Consequently, in the next step of development of our ps-PAAQ nanoparticles, after loading of the nanoparticles with the target mRNA, we have shielded their positive surface charge by coating the surface by electrostatic adsorption with two different block copolymers, composed of a negatively charged polyglutamic acid (PGA) block of 7.5 kD combined with a PEG block of 2 kD or 5 kD. The novel platform was analyzed both *in vitro* and *in vivo*, by testing the transfection efficiency in mammalian cell cultures and the local delivery of luciferase-expressing mRNA in mice.

In the following sections, the details in the development, physicochemical and biological properties of this new class of ps-PAAQ-based NPs are presented.

2. Materials and methods

2.1. Synthesis of the ps-PAAQ polymers

The ps-PAAQ (or p(CBA-ABOL-Q)/PEI) was synthesized by Michael-type polymerization of primary amines with bis(acrylamide)s as based on the procedure described by Lin et al. [10]. Other chemicals were purchased and used without further purification from Sigma-Aldrich or Avantor. A typical synthesis of one of the polymers is described below.

In brief, a small round-bottom flask was charged with 4-aminobutanol (**ABOL**) (0.60 g, 6.73 mmol), cystamine bis(acrylamide) (**CBA**) (2.60 g, 10 mmol), and N1-(7-chloroquinolin-4-yl)-hexane-1,6-diamine (**Q6**) (0.60 g, 2.16 mmol). MeOH (10 mL) was added, followed by a solution of $CaCl_2$ (0.44 g, 4 mmol) in water (2 mL). The resulting suspension was heated to 50 °C and was allowed to stir for an additional 48 h resulting in a nearly translucent solution (PAAQ polymer). A solution of branched PEI800 (Sigma-Aldrich M_n 600, 100 mg/mL in water, 680 μL) was then added and the reaction mixture was allowed to stir for another 72 h with heating. The reaction was subsequently terminated by acidification to pH 4 using hydrochloric acid and the resulting solution was transferred directly into a dialysis membrane (Spectrapor 6, 10 kD MWCO) for purification, where the polymer was dialyzed extensively against water. Then, the material was filtered through a 0.45 μm filter (cellulose acetate) and ultimately lyophilized to yield the branched ps-PAAQ polymer as a (hygroscopic) white solid.

For the transfection experiment testing different concentrations of Q in the ps-PAAQ polymer, the respective amounts of ABOL and Q used in the synthesis are shown in Table 1 with the other reagents, catalyst and solvents scaled linearly. In all other experiments, a concentration of 25 % Q in the polymer was used.

The ^{1}H spectra of the synthesized ps-PAAQs (in DMSO) were

Table 1
Amounts of CBA, ABOL and Q in the different tested polymers.

Polymer	CBA (mmol)	ABOL (mmol)	ABOL (%)	Q (mmol)	Q (%)
1	5.00	4.16	92.5	0.34	7.5
2	5.00	3.83	85	0.68	15
3	5.00	3.38	75	1.13	25
4	5.00	2.93	65	1.58	35
5	5.00	2.25	50	2.25	50

recorded on either a Bruker 400 MHz spectrometer or a Bruker 500 MHz spectrometer. The integrals exclusively corresponding to Q (in the aromatic region) were compared with the integral of the alkyl moieties in the 1–2 ppm range to measure the Q content in the purified polymers.

The molecular weight and polydispersity of the ps-PAAQ polymers and reference ps-PAA polymer without Q were determined by GPC relative to dextran standards (Sigma Aldrich). In short, GPC measurements were performed using a LC-40 system equipped with RID-20A detector (Shimadzu Europe GmbH). GPC measurements were performed using three CTO-40C thermostated (35 °C) columns serially connected (NOVEMA MAX Medium combination with a molar mass range: 100–1,000,000 Da; PSS NOVEMA Max 30 Å, 5 μm, 8 × 300 mm + 2 × NOVEMA Max 1000 Å, 5 μm, 8 × 300 mm, PSS Polymer Standards Service GmbH) with 100 mM NaCl + 0.3 % Formic acid as eluent at a flow rate of 1 mL/min.

2.2. Nanoparticle formulation and physicochemical characterization

For *in vitro* experiments, nanoparticles were formed by first preparing a solution of 120 μg/mL of mRNA encoding EGFP (CleanCap®, TriLink Biotechnologies) in 10 mM Histidine 10 % Trehalose buffer at pH 6.5. In addition, the ps-PAA polymers, with or without Q, were dissolved at a concentration of 3 mg/mL in 10 mM Histidine 10 % Trehalose buffer at pH 6.5. The 120 μg/mL solution of mRNA was added 1:1 *v*/v to the cationic polymers. After mixing, the solutions were incubated for at least 15 min at room temperature before storage in the freezer. In all formulations, the resulting polymer-to-mRNA ratio was 25:1 *w*/w (1.5 mg/mL of PNP to 60 μg/mL of mRNA).

For *in vivo* experiments a higher nanoparticle concentration is used, therefore the final formulations had 5 mg/mL of PNP and 200 μg/mL of mRNA. In this case, as a payload we used firefly luciferase mRNA (CleanCap®, TriLink Biotechnologies).

To obtain polyglutamic acid – polyethylene glycol (PGA-PEG) coated nanoparticles, the coating material ($mPEG_{2k}$-b-PLE_{50} or $mPEG_{5k}$-b-PLE_{50}, Alamanda Polymers) was added to the mRNA solution in the first step, which was then added to the polymers in the same mixing step. Different coating-to-polymer weight ratios were tested according to the A/N charge ratio and coating type. The A/N ratio is defined here as the molar charge ratio of the anionic block copolymer used as a coating (PGA-PEG) to the cationic poly(amidoamine) polymer. The A/N ratio 1.0 is the case when the total charge density of the nanoparticle is neutral. To illustrate this calculation for the $PGA_{7.5k}$-PEG_{5k} coating: the PGA-PEG has 1 charge per *ca.* 250 Da, and the cationic polymer has 1 charge per *ca.* 400 Da, then at the A/N ratio 1.0 this would result in a coating-to-polymer *w*/w ratio of 250/400 = 0.6.

The resulting nanoparticle size, zeta potential and polydispersity index were measured using Dynamic Light Scattering (DLS) in the Zetasizer Nano ZS90 (Malvern), with a 90-degree scattering optics. Samples were diluted 5-fold in 10 mM Histidine 10 % Trehalose buffer (pH 6.5), then loaded in a disposable plastic micro cuvette (ZEN0118, Malvern) for measurements. Results were analyzed in the Zetasizer software (version 7.13, Malvern).

2.3. RiboGreen assay for mRNA quantification

We developed a protocol to quantify the EGFP mRNA released by the nanoparticles with increasing heparin concentrations, as well as to estimate the encapsulation efficiency of the mRNA-PNP formulations. Loaded nanoparticles (1.5 mg PNP/mL) were diluted 1:100 in 250 mM histidine pH 7.2 (dilution buffer) to a final concentration of 15 μg/mL. For the release assay, 50 μL of these nanoparticles were further diluted with 50 μL of 0–8 μg/mL heparin in a 96-well plate, until 0–4 μg/mL final heparin concentrations. Following incubation for 30 min at 37 °C to allow the release, we added to each well 50 μL of RiboGreen reagent (Invitrogen) diluted 2000-fold with the dilution buffer. After brief shaking and 5-minute incubation at room temperature, fluorescence was measured at excitation/emission of 480/530 nm in a microplate reader (Tecan Infinite M200 Pro). For the encapsulation assay, the free mRNA (not encapsulated) was measured in fresh mRNA-PNP formulations diluted 1:10 in the dilution buffer, then directly incubated with RiboGreen reagent as above. Measurements were corrected for preparations containing empty nanoparticles (without mRNA payload). The concentration of released (or free) mRNA was measured using a calibration curve of free EGFP mRNA (TriLink Biotechnologies) and expressed as a percentage of total mRNA present.

2.4. Gel electrophoresis for mRNA stability

Coated and uncoated nanoparticles were loaded with EGFP mRNA in 10 mM Histidine 10 % Trehalose buffer (pH 6.5), and aliquots were incubated for 1, 2, 5, 7, 9 and 14 days at 37 °C. Loaded nanoparticles in buffer solution, stored in the freezer at −80 °C, were also tested in this experiment (day 0). The integrity of mRNA from loaded PNPs was verified by agarose gel electrophoresis, using 1 % agarose gel and SYBR® Safe DNA Gel Stain (Invitrogen) for visualization of the mRNA under UV light. Before the assay, the mRNA-loaded nanoparticles were treated for 5 min at 60 °C with 2 M 1,4-Dithiothreitol (DTT; Sigma-Aldrich) and 5 mg/mL heparin (Sigma-Aldrich) to release the cargo by reduction and displacement. Gel electrophoresis was performed for 30 min at 100 V and visualized using a ChemiDoc Imaging System (Bio-Rad). If any mRNA was degraded during the stability study, it will appear as a smear in the gel, while clear and well-defined bands indicate mRNA intactness.

2.5. Cell culture

Immortalized COS-7 monkey kidney fibroblasts were cultured in a growth medium composed of Dulbecco's modified Eagle's medium (DMEM, high glucose, pyruvate; Gibco), supplemented with 10 % *v*/v fetal bovine serum (FBS; Biowest) at 37 °C under a humidified 5 % CO_2 atmosphere. Immortalized C_2C_{12} mouse myoblasts were cultured in growth medium composed of DMEM supplemented with 20 % *v*/v FBS, under the same incubation conditions. Medium changes were performed every 2–3 days and cells were passaged at 70–90 % confluency in 75 cm^2 T-flasks.

2.6. Delivery of mRNA using nanoparticles

COS-7 cells were seeded in 48-well cell culture plates (1.6×10^4 cells/cm^2) in culture medium DMEM with 10 % v/v FBS, in triplicate per condition and with a final volume of 200 μL. C_2C_{12} cells were seeded in 96-well plates (6×10^3 cells/cm^2), under the same culture conditions. Twenty-four hours after seeding the cells, the medium was replaced by the same volume of NP solutions diluted to the required concentrations for transfection, in DMEM with 10 % *v*/v FBS additionally buffered with 20 mM HEPES (Gibco). Transfections were performed in COS-7 cells with NP formulations at an mRNA dose of 0.6 μg/mL. For C_2C_{12} cells, the concentration of mRNA in transfections ranged from 0.5 to 6.0 μg/mL. After incubation for 24 h, viability testing and flow cytometry were performed. The transfection reagent jetMESSENGER® (Polyplus) was used as a positive control for mRNA transfections, following the manufacturer's protocol.

2.7. Metabolic activity and toxicity screening

The alamarBlue™ assay was used to determine the metabolic activity 24 h after transfections in COS-7 cells (same seeding conditions as above). For each sample, the culture medium was aspirated and replaced with same volume of DMEM containing 10 % *v*/v of Resazurin solution at 440 mM (Sigma-Aldrich). After 4 h under standard cell culture conditions (37 °C and 5 % CO_2), 100 μL of each sample was transferred to a transparent 96-well plate and had the fluorescence measured in a

microplate reader (Tecan Infinite M200 Pro) at excitation/emission of 560/590 nm. A blank group was also included in the experiment with working solution only (DMEM with 10 % *v*/v Resazurin). Triplicates were averaged, wells were corrected for the average medium fluorescence by subtraction of the blank values, and metabolic activity was determined by the percentage of Resazurin reduction in relation to untreated cells.

2.8. Flow cytometry

Cells were trypsinized with 50 μL of Trypsin-EDTA (0.25 %) per well and incubated for 3 min at 37 °C. Then, 200 μL of DMEM with 10 % *v*/v FBS was added to each well and the cells were resuspended. A final volume of 100 μL per sample was transferred to a 96-well plate and kept on ice until measurement was performed in a MACSQuant® flow cytometer (Miltenyi Biotec). Forward, side scatter, and laser voltage were adjusted using untreated cells.

2.9. In vivo testing of PNPs

2.9.1. Animals and experimental design

Animal procedures were performed at University of Twente (Netherlands), under license number AVD11000 2018 6524. Ten-week-old female BALB/c mice were purchased from Janvier Labs (France) and acclimatized for one week before experiments were started. The animals were housed in cages of five subjects per group and had *ad lib* access to water and food.

2.9.2. Intramuscular delivery of PNPs with luciferase mRNA in mice, imaging of bioluminescence and luciferase detection in muscle homogenates

In a first experiment, we evaluated luciferase signal detection in muscle tissue homogenates. For intramuscular (IM) delivery, 50 μL of the NP formulations (=10 μg of mRNA) were injected into each hind limb with a 26G needle, in the biceps femoris muscle. Mice were euthanized by cervical dislocation after 24 h, and tissue samples of the injected muscles were collected. Luciferase activity and protein content were determined in muscle homogenates. For this, 600–900 μL of luciferase cell culture lysis buffer (Promega) and 1.4 mm ceramic beads (Qiagen) were added to muscle tissue samples of known weight (200–300 mg). The samples were homogenized with a BeadBug™ microtube homogenizer (Sigma-Aldrich) for 90 s, 4000 rpm at 4 °C. After homogenization, the samples were centrifuged 10 min at 10,000 ×*g* at 4 °C. The obtained supernatant was used for further analysis of the luciferase activity. Bio-Glo™ Reagent (Promega) was used to quantify the luciferase activity in the supernatant of the muscle homogenates. Total protein was measured in the supernatant using a Bradford protein assay (Bio-Rad). The luciferase activity was expressed as relative luminescent units (RLU) per mg of protein in the samples.

In a second experiment, the luciferase activity in mice was measured by whole body imaging. This was done 24 h after intramuscular (IM) injection of 25 μL of the NP formulations (=5 μg of mRNA) into each hind limb with a 26G needle. The animals were injected in the gastrocnemius muscle. Whole body imaging of the chemiluminescence was performed 10 min after intraperitoneal luciferin injection (250 μL of 12 mg/mL D-luciferin in DPBS). Before imaging, mice were euthanized by cervical dislocation, and the skin from the legs was removed for imaging purposes. The Pearl® Trilogy Imaging System was used for the measurement of bioluminescence, using standard settings. Quantification of the luciferase intensity was performed using the Image Studio software (version 5.2).

2.10. Statistics

Statistical analyses were performed using GraphPad Prism (version 9.3.1; GraphPad® Software). Two-Way ANOVA with Bonferroni multiple comparison test was performed to know how polymer type and heparin concentration affected mRNA release from nanoparticles. In the analysis of luciferase activity in tissue homogenates, we used One-Way ANOVA with Tukey's multiple comparison test. The readouts from both hind limbs of the same animal were considered technical replicates and results were averaged before statistical analysis. In the imaging of luciferase bioluminescence in mice, we used unpaired *t*-test with Welch's correction. Values of $p \leq 0.05$ were considered to be statistically significant. All data are shown as mean ± standard deviation.

3. Results

3.1. Synthesis of the ps-PAAQ polymers

Two monomers were made for the synthesis of the polymers. The first monomer, cystamine bis(acrylamide) (CBA), was synthesized as described by Lin et al. [10]. The second monomer, N1-(7-chloroquinolin-4-yl)-hexane-1,6-diamine (Q6), was synthesized analogously to the described synthesis by Natarajan et al. [36]. Fig. 1 illustrates the synthesis of these ps-PAAQ polymers, which is further described hereafter. A mixture of two amine-containing building blocks, Q6 and 4-aminobutanol (ABOL), are used to generate a random PAAQ *co*-polymer with the CBA.

This polymerization takes place *via* an Aza-Michael reaction in a polar protic solvent system suitable for this type of reaction. A calcium chloride catalyst was used as it was previously found to enhance the reaction rate substantially resulting in a shorter reaction time [37]. After 48 h, oligomeric ethyleneimine (PEI800) was added in a one-pot reaction, yielding branched ps-PAAQ polymers.

Six different ps-PAAQ polymers with different Q concentrations in the side chains were synthesized *via* Michael addition of the corresponding primary amine monomers to cystamine bis(acrylamide). The ^{1}H NMR spectra of the polymers were in full accordance with the expected structures. The amount of Q in the purified polymers could be measured by NMR comparing the aromatic Q proton integrals (integral at 6.8 ppm set to 1) with the alkyl chain integral at 1.2–1.8 ppm:

$$Ratio\ ABOL\ to\ Q6 = \frac{[\text{Integral 1.2–1.8 ppm}]-8}{4}$$

The Q content corresponded well to the feedstock of the polymerization (Table 2), indicating the successful incorporation of both monomers in the polymer and retention of both during the purification process.

Gel permeation chromatography (GPC) measurements showed that the weight-average molecular weights (Mw) of these ps-PAAQ polymers were in the range from 8000 to 40,000 g/mol (Table 2). An increase of the Q content led to an observed eluting behavior corresponding to a lower molecular weight of the dextran standard. It is not clear whether the hydrophobic character of the Q building block leads to a more compact (globular) structure of the ps-PAAQ polymer or polymers with an overall lower molecular weight are predominantly formed.

3.2. Coating of ps-PAAQ nanoparticles with a PEG-polymer for particle shielding and improved stability

The potential benefits of the electrostatic adsorption of block copolymers were investigated with the aim to shield the positive surface charge of the ps-PAAQ NPs. These copolymers are composed of poly L-glutamic acid (PGA) and a polyethylene glycol (PEG) chain of different molecular weights. Earlier work in our laboratory has indicated that a PGA length of 7.5 kD was sufficient to form a stable interaction with the cationic PNPs, while longer lengths were more prone to induce aggregation (data not shown). Here, two types of coatings were evaluated, differing from each other by the length of the PEG chain: $PGA_{7.5k}$-PEG_{2k} or $PGA_{7.5k}$-PEG_{5k}. The coating-to-polymer weight ratios tested for physicochemical characterization of mRNA-loaded nanoparticles may also be expressed as the "A/N ratio" for each of the coatings (Fig. 2). The

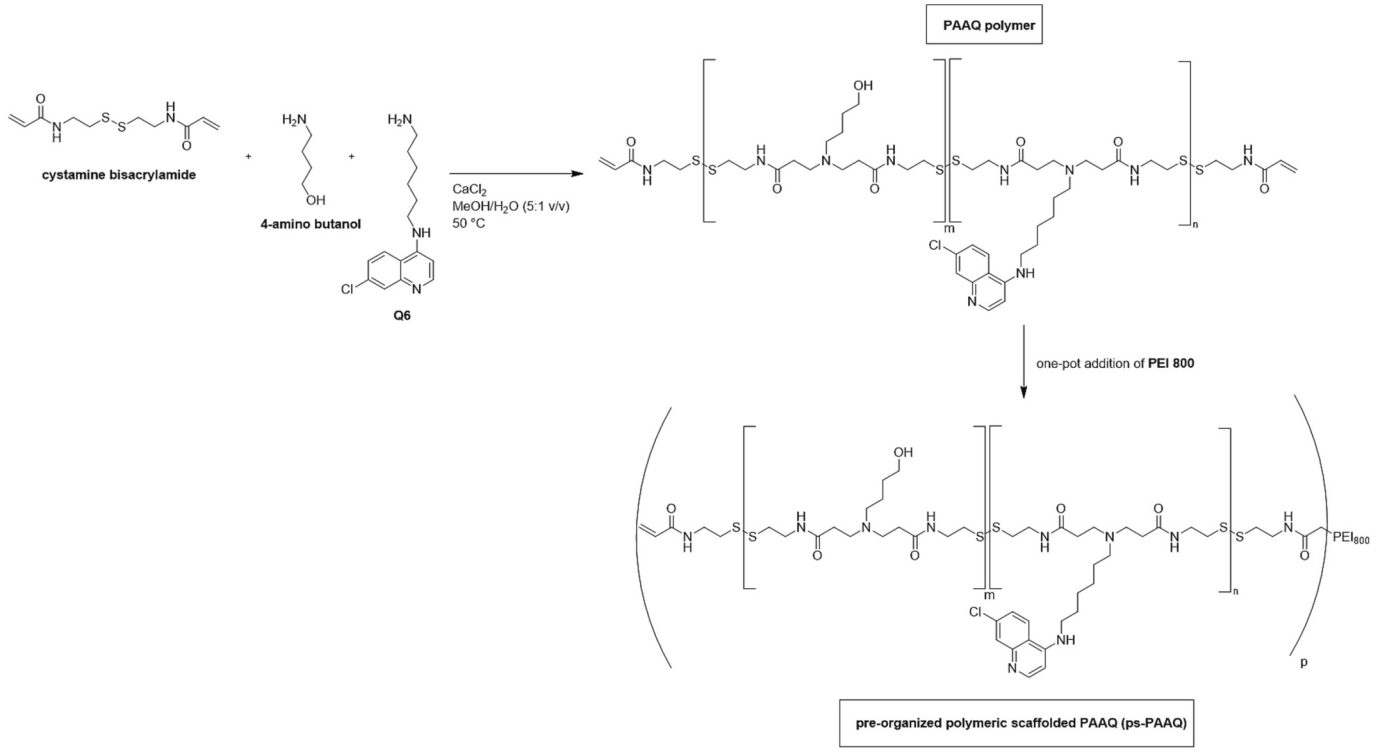

Fig. 1. Synthesis of the pre-organized polymeric scaffolded PAAQ (ps-PAAQ). Q6 = N1-(7-chloroquinolin-4-yl)-hexane-1,6-diamine; PAAQ = poly(amidoamine) with incorporated Q6 building block as well as 4-aminobutanol; PEI800 = oligomeric branched ethyleneimine (Mw ~800, Mn ~600).

Table 2
Characteristics of ps-PAAQ polymers: NMR characterization of Q content *versus* feedstock (theoretical), Number-Average Molecular Weight (Mn), Weight-Average Molecular Weight (Mw), and Mw/Mn Ratio (PDI).

Polymer	Q % of monomers (theoretical)	Integral NMR (1.2–1.8 ppm)	Q % of monomers (derived from NMR integral)	Mn	Mw (kDa)	Mw/Mn (PDI)
1	0.0 %	0.00	0.0 %	10.5	39.7	3.78
2	7.5 %	59.56	7.2 %	9.6	27.8	2.90
3	15.0 %	29.37	15.8 %	7.8	19.8	2.54
4	25.0 %	20.05	24.9 %	5.4	15.3	2.83
5	35.0 %	15.55	34.6 %	4.0	11.9	2.98
6	50.0 %	12.26	48.4 %	2.0	8.3	4.15

A/N ratio is defined here as the molar charge ratio of the anionic block copolymer used as a coating (PGA-PEG) to the cationic poly(amidoamine) polymer. Importantly, the A/N ratio 1.0 is obtained when the net charge of the nanoparticle formulation is approximately neutral, and which is similarly expected to result in near-neutral surface charge of the NPs. This condition corresponds to 0.5 *w*/w coating-to-polymer ratio for the $PGA_{7.5k}$-PEG_{2k} coating, and to 0.6 *w*/w coating-to-polymer ratio for the $PGA_{7.5k}$-PEG_{5k} coating (Fig. 2).

After formulation of the different ps-PAAQ NPs, the average size (*Z*-Average), polydispersity index (PDI) and zeta potential of nanoparticles were measured in the buffer solution (10 mM Histidine and 10 % Trehalose, pH 6.5). Fig. 2 shows the results of DLS measurements for the $PGA_{7.5k}$-PEG_{2k} and $PGA_{7.5k}$-PEG_{5k} coatings. As a control, we also included in these experiments the mRNA-loaded ps-PAAQ without PGA-PEG coating (referred here as "uncoated NPs"). These uncoated NPs showed average size around 75 nm and PDI values above 0.2.

The PGA-PEG coating with PEG length 5kD effectively shielded the charge of the nanoparticles in buffer. This coating produced nanoparticles with a neutral surface charge between −5 and +5 mV (Fig. 2D), showing more positive values as the coating-to-polymer weight ratio decreases. As expected, uncoated NPs showed a strong positive surface charge between +18 and +26 mV (Fig. 2B, D). The average particle size was around 50 nm for all coating-to-polymer ratios, and PDI values were smaller than 0.1 for all coating-to-polymer ratios higher than 0.2 *w*/w (Fig. 2C).

The other PEG chain tested (PEG_{2k}) proved to be too short to shield the nanoparticles to the same extent as PEG_{5k} (Fig. 2A). The average size and PDI values were considerably higher with this coating for all PGA-PEG to polymer ratios, and it was less efficient in shielding the positive charges of the nanoparticles in most of the coating-to-polymer ratios (Fig. 2B). The A/N charge ratio 1.0, in which the charge density of nanoparticles becomes neutral, was the worst-case scenario showing very high polydispersity (PDI ~1.0) and indicating complete heterogeneous size distribution, likely due to aggregation of the particles at near-neutral surface charge. This effect, however, was not observed for the $PGA_{7.5k}$-PEG_{5k} coating, further supporting its efficiency as a shielding group. Indeed, these nanoparticles showed a highly homogeneous size distribution (Fig. S1). Based on these results, the PEG_{5k} was chosen for further testing in this work.

To investigate the effects of the coating on the stability of mRNA in the nanoparticles, ps-PAAQ NPs loaded with EGFP mRNA were coated with $PGA_{7.5k}$-PEG_{5k} in a 1:1 *w*/w ratio and compared to uncoated nanoparticles. The thermostability of the encapsulated mRNA was determined by agarose gel electrophoresis. The nanoparticles were kept in a buffer solution of 10 mM Histidine and 10 % Trehalose (pH 6.5) for 1, 2, 5, 7, 9 and 14 days at 37 °C. Loaded nanoparticles in buffer solution and stored at −80 °C were included in this experiment as a stable control ("0 day" incubation). The results shown in Fig. 3 illustrate that coated ps-PAAQ NPs were more efficient in protecting the mRNA payload from degradation over time. The first signs of mRNA degradation were observed after 14 days of incubation at 37 °C, whereas uncoated ps-PAAQ NPs showed complete mRNA degradation after 5 days of incubation indicated by the "smearing" of mRNA on the gel. This result suggests an evident advantage of the $PGA_{7.5k}$-PEG_{5k} coating of the

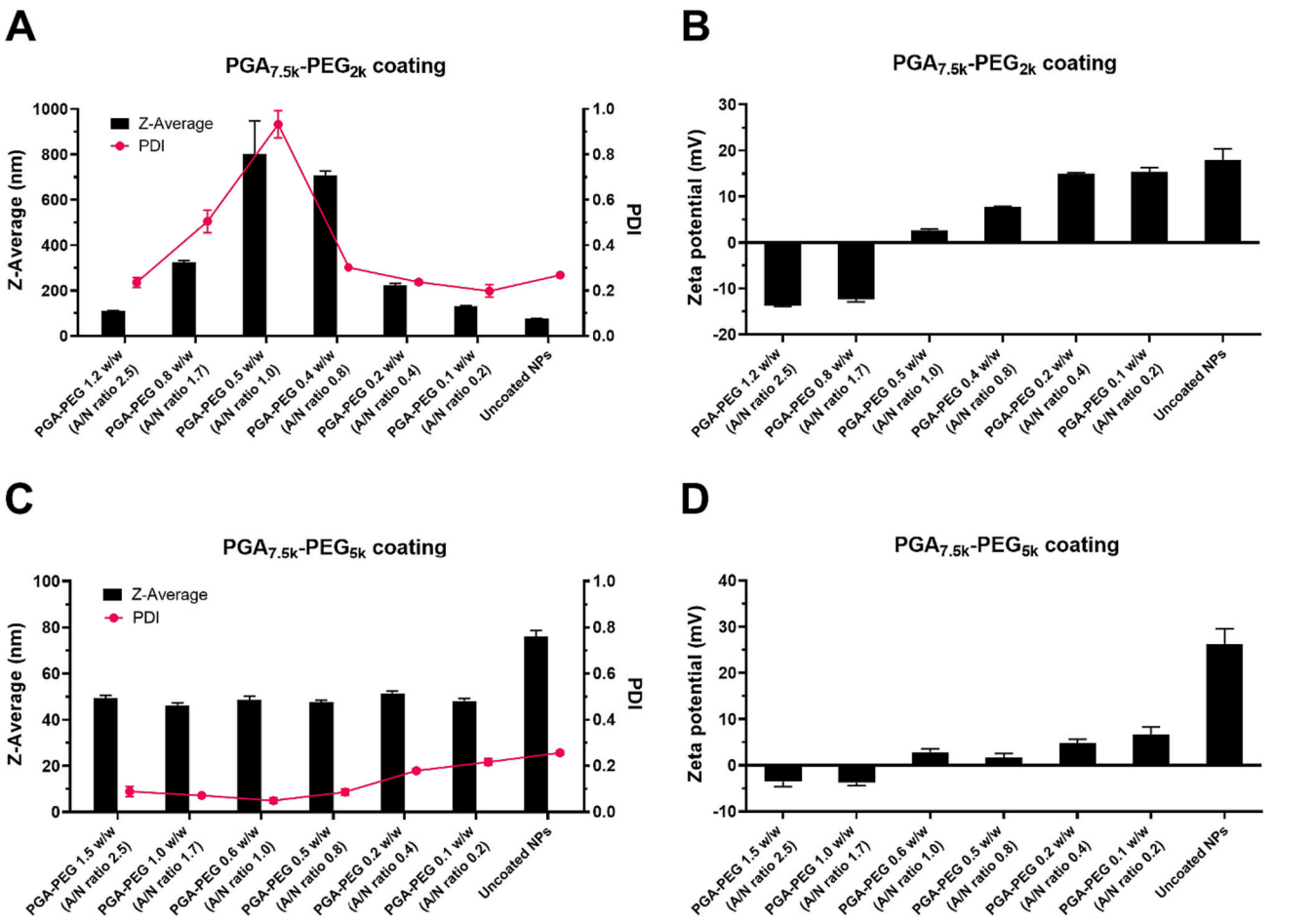

Fig. 2. Particle size and surface charge results of $PGA_{7.5k}$-PEG_{2k} and $PGA_{7.5k}$-PEG_{5k} at different coating/ps-PAAQ polymer weight ratios. The respective A/N molar charge ratios are also indicated. (A) Average size and PDI results for the $PGA_{7.5k}$-PEG_{2k} coating. (B) Zeta potential results for the $PGA_{7.5k}$-PEG_{2k} coating. (C) Average size and PDI results of nanoparticles for the $PGA_{7.5k}$-PEG_{5k} coating. (D) Zeta potential results of nanoparticles for the $PGA_{7.5k}$-PEG_{5k} coating. Measurements were performed with ps-PAAQ nanoparticles diluted in buffer solution (10 mM Histidine 10 % Trehalose, pH 6.5). Results are the combined data of three individual measurements.

cationic mRNA-loaded ps-PAAQ nanoparticles as a means to improve the mRNA thermal stability.

3.3. *Effect of Q on the stabilization of mRNA-loaded ps-PAAQ NPs*

In this experiment, a polymer incorporating only the ABOL monomer without Q was synthesized (ps-PAA). This polymer formed NPs after loading with EGFP mRNA, having a particle size of 80.5 ± 1.5 nm for uncoated ps-PAA NPs and 62.4 ± 1.8 nm for PEG-coated ps-PAA NPs. Together with the standard ps-PAAQ NPs (containing 25 % of Q), they were used in a release assay with heparin competition to displace the mRNA from the nanoparticle. Because heparin has a high density of negative charges, it can compete with the mRNA for the binding to the cationic core of the polymer and release mRNA from the PNPs. We developed a protocol to quantify the released mRNA using the RiboGreen assay, by competition with increasing heparin concentrations. The results in Fig. 4A show that mRNA release was significantly higher with uncoated ps-PAA NPs for all heparin concentrations tested, achieving 33 % in the presence of 4 μg/mL heparin compared with 12 % for Q-containing NPs. For PEG-coated ps-PAA NPs, a similar behavior was observed with even more significant differences at lower heparin concentrations (Fig. 4B). Compared with uncoated ps-PAA NPs, the lower mRNA release from coated ps-PAA NPs at the highest heparin concentration (4 μg/mL) might be explained by the shielding effect provided by the $PGA_{7.5k}$-PEG_{2k} coating.

The lower release of mRNA from ps-PAAQ nanoparticles indicates a stronger interaction between the Q-containing polymer and the mRNA. Indeed, for ~12 % release the uncoated ps-PAAQ NPs require a two times higher heparin concentration (4 μg/mL) to achieve the same level of mRNA release compared to ps-PAA NPs (2 μg/mL of heparin) (Fig. 4A). These results show that the presence of Q in the nanoparticle scaffold is clearly contributing to the stability of the mRNA-loaded nanoparticle. This stabilization is especially evident for the ps-PAAQ NPs coated with PGA-PEG, when no heparin is added (Fig. 4B). As the coating is *co*-formulated with the mRNA and the PAA-based polymer in the same mixing step, in the absence of Q it is possible that a fraction of this mRNA is displaced by the anionic PGA-PEG during loading into the NPs. The Q-containing polymer, on the other hand, shows significantly lower levels of mRNA release regardless of the PGA-PEG addition in the NP formulation.

We also quantified the encapsulation efficiency of both ps-PAA and ps-PAAQ NPs by the RiboGreen assay, by indirect measurement of free EGFP mRNA in fresh formulations of mRNA-PNPs. As a result, for uncoated NPs we obtained excellent loading efficiencies of 99.98 ± 0.15 % for ps-PAA and 99.82 ± 0.68 % for ps-PAAQ. For coated NPs, the loading efficiency was also high for the Q-containing polymer (ps-PAAQ, 98.93 ± 0.05 %), but lower for the polymer without Q (ps-PAA, 91.14 ± 0.39 %). This amount of free mRNA detected in coated ps-PAA NPs (~10 %) corroborates the result observed in Fig. 4B in the condition where no heparin was added.

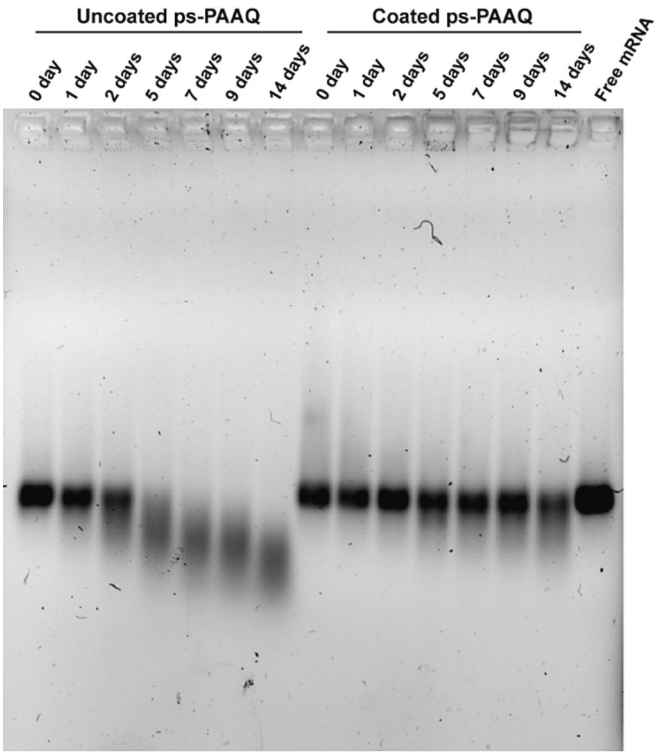

Fig. 3. mRNA stability of uncoated *vs* coated ps-PAAQ NPs in agarose gel electrophoresis. Coating of NPs with $PGA_{7.5k}$-PEG_{5k} was done in a 1:1 *w*/w ratio. The formulations were incubated at 37 °C during the indicated days and "day 0" are samples taken directly from the −80 °C storage. A free EGFP mRNA control group (60 μg/mL) was used as a reference.

3.4. *In vitro transfection efficiency of PAA-based NPs with increasing quantities of Q*

To demonstrate the effect of increasing Q concentrations in the polymers on the transfection efficiency, ps-PAAQ polymers were synthesized with increasing amounts of Q, ranging from 7.5 to 50 mol% of the amine monomers (Table 1). Different formulations loaded with EGFP mRNA were made from these polymers and used in transfections of COS-7 cells, which are easy to manipulate and widely used for the expression of exogenous genes or proteins. The formed nanoparticles were characterized by DLS as shown in Table S1.

The transfection efficiency and cell viability following 24 h of incubation of COS-7 cells with mRNA-loaded nanoparticles are shown in Fig. 5. The percentage of GFP-positive cells clearly increased with increasing amounts of Q in the polymers, with a maximum efficiency of *ca.* 81 % of transfected cells obtained with polymers containing 50 % Q. The cell viability showed an opposite trend (Fig. 5), with a marked drop going from 25 % to 35 % Q in the ps-PAAQ polymer. For Q concentrations up to 25 % in the polymer, the percentage of viable cells remained unchanged in relation to untreated cells (>98 %). The optimal Q concentration in the polymer was considered to be 25 % Q, showing a combination of high transfection efficiency without significant reduction of cell viability. Therefore, for all the biological experiments described in the next sections nanoparticles containing 25 % Q in the polymer (ps-PAAQ) were used.

3.5. *Dose-dependent toxicity of PAA-based NPs in C_2C_{12} cells*

To further evaluate the cytotoxicity of the polymers, we performed transfection experiments in C_2C_{12} mouse muscle cells, a relevant cell type for testing the intramuscular application of our technology. Here, the polymer containing 25 % of Q (ps-PAAQ) was compared to the polymer without Q (ps-PAA) after loading with EGFP mRNA. For a clear dose-response evaluation, we tested concentrations ranging from 0.5 to 6 μg/mL of mRNA. For concentrations up to 4 μg/mL, cell viability was >95 % for transfections with both nanoparticle types (Fig. 6). A toxic effect could be observed mainly for ps-PAAQ NPs at higher mRNA concentrations (≥5 μg/mL), showing a cell viability gradually lower than 80 %. Importantly, our platform showed to be less toxic than the positive control jetMESSENGER® (cell viability = 79 ± 6 %). Together, these results support the biocompatibility of these PAA-based NPs for *in vitro* transfection of mammalian cells.

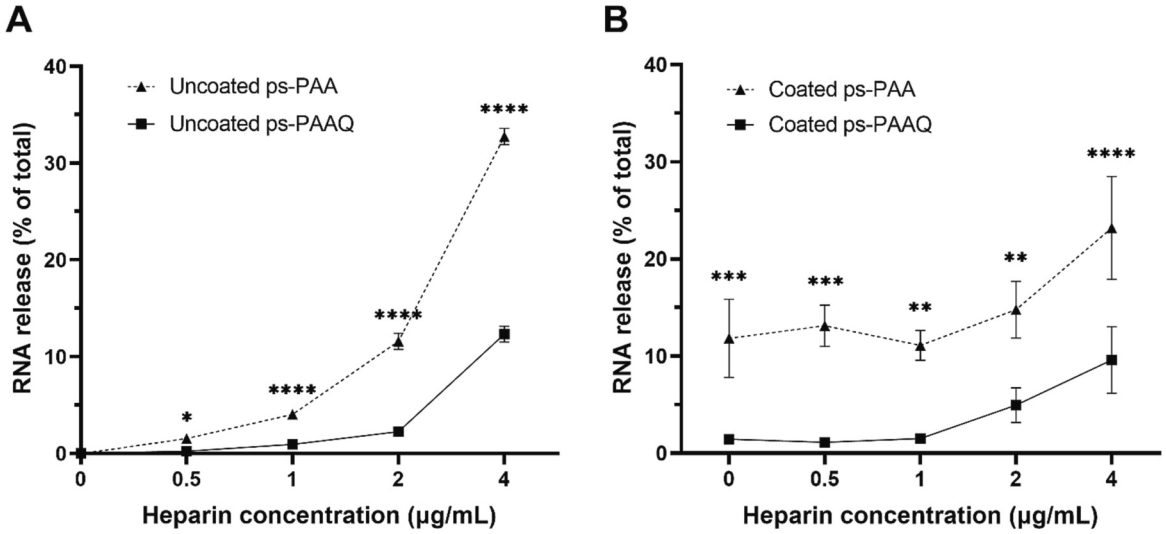

Fig. 4. Heparin competition assay for EGFP mRNA release from PAA-based NPs. (A) Comparison between uncoated nanoparticles based on ps-PAA, a polymer without Q, and ps-PAAQ, a polymer containing 25 % of Q. (B) Comparison between PEG-coated nanoparticles based on ps-PAA, a polymer without Q, and ps-PAAQ, a polymer containing 25 % of Q. Coating of NPs with $PGA_{7.5k}$-PEG_{5k} was done in a 1:1 *w*/w ratio. The mRNA release is measured with RiboGreen reagent after incubation of the nanoparticles with increasing concentrations of heparin, and is expressed as a percentage of total mRNA in the PNPs. Two-Way ANOVA with Bonferroni correction was used to compare "ps-PAA" *vs* "ps-PAAQ" at each heparin concentration ($n = 3$). Statistically significant difference is indicated by (*) to *p*-value ≤ 0.05, (**) to p-value ≤ 0.01, (***) to p-value ≤ 0.001, or (****) to p-value ≤ 0.0001.

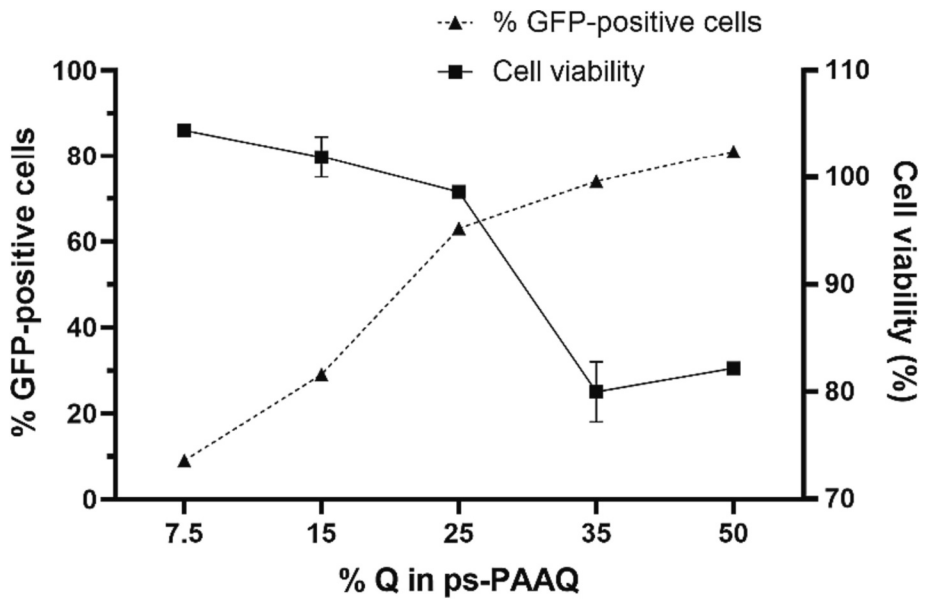

Fig. 5. Transfection efficiency and viability of ps-PAAQ NPs in COS-7 cells. Comparison of EGFP mRNA-loaded NPs with increasing concentrations of Q in the polymer (7.5 to 50 %). A single concentration of 0.6 μg/mL mRNA was used in transfections. The percentage of GFP-positive cells was determined by FACS after 24 h by the gating of live, single cell events. Cell viability was determined after 24 h by the AlamarBlue assay, in relation to untreated cells.

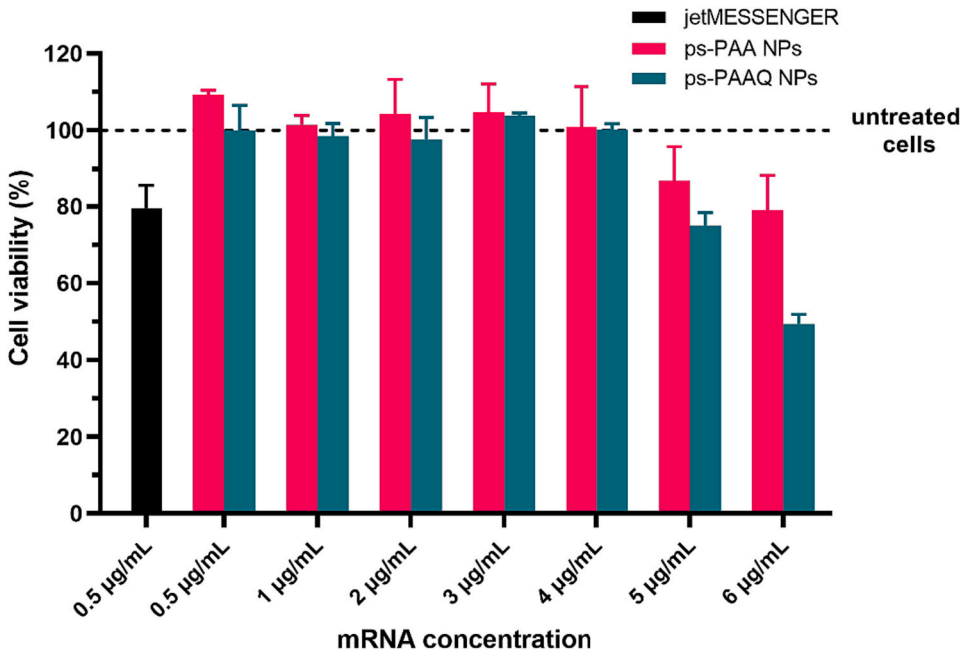

Fig. 6. Cell viability with PAA-based NPs in C_2C_{12} cells. Comparison between nanoparticles based on ps-PAA, a polymer incorporating only the ABOL monomer without Q, and ps-PAAQ, a polymer containing 25 % of Q. Cell viability was determined after 24 h by the AlamarBlue assay, in relation to untreated cells. The jetMESSENGER® mRNA transfection reagent was used as a positive control in transfections, following supplier's protocol.

3.6. Transfection efficiency of PAA-based NPs in C_2C_{12} cells

As a next step, we repeated the transfection experiments in C_2C_{12} mouse muscle cells to find out what nanoparticle type works better as a delivery system *in vitro*. Again, the polymer containing 25 % of Q (ps-PAAQ) was compared to the polymer without Q (ps-PAA) after loading with EGFP mRNA. We additionally tested ps-PAA and ps-PAAQ NPs coated with $PGA_{7.5k}$-PEG_{5k} in a 1:1 *w*/w ratio. Transfection efficiency was analyzed after 24 h by FACS and measured by percentage of GFP-positive cells. According to the cell viability results from the previous section, we chose a safe/non-toxic concentration range of 0.5 to 3 μg/mL mRNA.

As a result, it is possible to observe a dose-dependent response of GFP expression with increasing mRNA concentrations (Fig. 7). Indeed, the higher concentrations (2 and 3 μg/mL mRNA) showed the highest GFP levels for both uncoated and coated ps-PAAQ NPs (60–72 % of positive cells), with little difference regarding the coating presence. Beyond those concentrations, no improvement in gene expression was observed (data not shown). In contrast, for the most part, ps-PAA NPs induced remarkably lower levels of GFP-positive cells, regardless of the presence of PEG-coating. The transfection efficiency showed by these nanoparticles without Q was superior to 50 % only for the uncoated ps-PAA

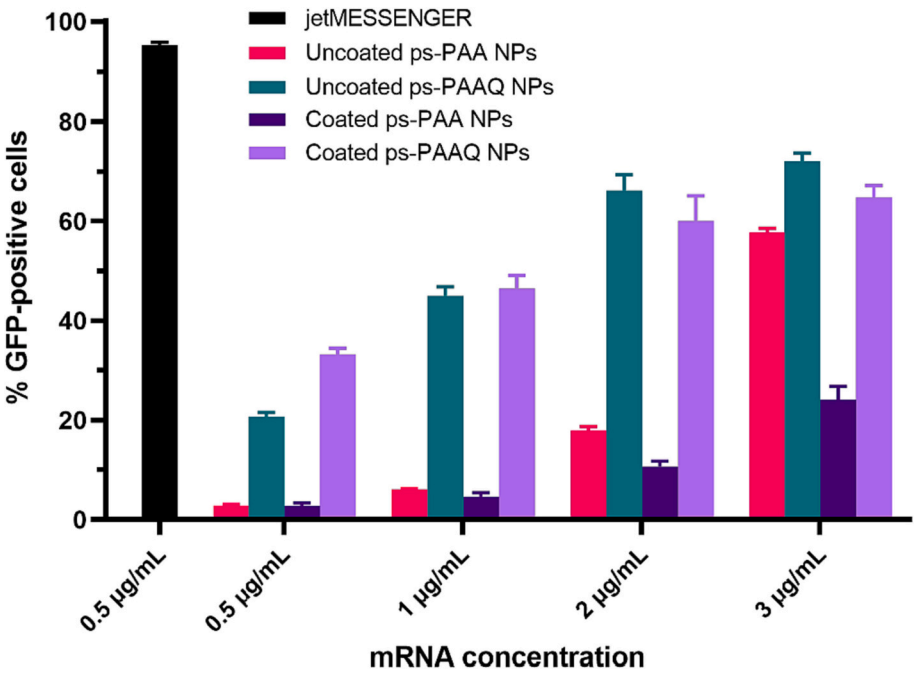

Fig. 7. Transfection efficiency of PAA-based NPs in C_2C_{12} cells. Comparison between uncoated and coated ps-PAA *vs* ps-PAAQ nanoparticles. Coating of PNPs with $PGA_{7.5k}$-PEG_{5k} was done in a 1:1 *w*/w ratio. The percentage of GFP-positive cells was determined by FACS after 24 h by the gating of live, single cell events. The jetMESSENGER® mRNA transfection reagent was used as a positive control in transfections, following supplier's protocol.

NPs at the highest mRNA concentration tested (3 μg/mL). Compared with the positive control mRNA transfection reagent jetMESSENGER® (>95 % GFP-positive cells), our platform had a satisfactory performance and lower toxicity (Fig. 6). Importantly, these results corroborate the advantage of having functional Q groups in the polymer backbone, as it indicates a clear effect in the enhancement of transfection efficiency *in vitro*.

3.7. Luciferase activity after intramuscular injection of ps-PAAQ NPs in mice

To evaluate *in vivo* different coating ratios and compare them with uncoated nanoparticles, the ps-PAAQ NPs were *co*-formulated with different amounts of $PGA_{7.5k}$-PEG_{5k} and loaded with luciferase mRNA for intramuscular injection in mice. The luciferase expression was quantified in tissue homogenates and the results of this study are summarized in Fig. 8.

Three coating ($PGA_{7.5k}$-PEG_{5k}) to polymer (ps-PAAQ) ratios were compared in these studies: 0.125:1, 0.5:1 and 1:1 *w*/w. Luciferase expression was detectable 24 h after treatment in muscle tissue from all injected groups (Fig. 8). The $PGA_{7.5k}$-PEG_{5k} coated NPs in a 1:1 *w*/w ratio induced a significantly higher luciferase activity than uncoated NPs and the other coated formulations, as detected in the tissue homogenates. The formulations with lower coating-to-polymer ratios (0.125:1 and 0.5:1 *w*/w) showed an increasing trend of luciferase activity compared with the uncoated NP control group, even though this was not statistically significant (Fig. 8). As an additional proof-of-concept of the advantage of Q incorporation in the polymer, we compared the nanoparticles of ps-PAAQ, with 25 mol% Q in the side chains, and nanoparticles of ps-PAA, without Q in the composition. Both nanoparticles were also coated with $PGA_{7.5k}$-PEG_{5k} at a 1:1 *w*/w coating-to-polymer ratio. Only background signal was detected in the animals treated with PAA-based NPs (Fig. 8). The amount of luciferase in muscle homogenates was significantly higher in ps-PAAQ NP treated mice compared with ps-PAA NPs. These results corroborate the *in vitro* findings in C_2C_{12} cells (Fig. 7) and provide additional evidence to support the incorporation of Q in the polymers.

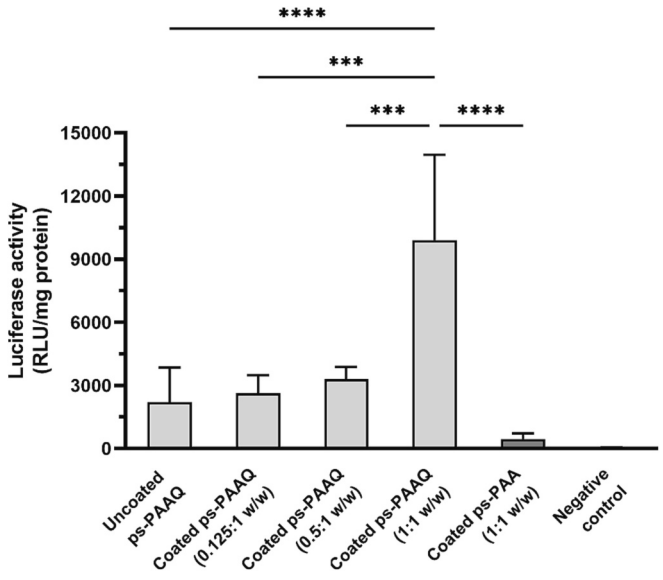

Fig. 8. Luciferase expression in muscle homogenates, after intramuscular (biceps femoris) injection of PNPs loaded with luciferase mRNA. Quantification of luciferase activity was performed in muscle homogenates 24 h after treatment with PAA-based NPs with the indicated $PGA_{7.5k}$-PEG_{5k} coating/PAA polymer weight ratios. Negative control refers to animals that received NP injection in the biceps femoris but had the muscle from the fore limbs collected for tissue analysis. $n = 5$ animals per group, One-Way ANOVA with Tukey's multiple comparison test. Statistically significant difference is indicated by (***) to *p*-value ≤ 0.001, or (****) to p-value ≤ 0.0001. RLU = relative light unit.

The higher luciferase expression with 1:1 *w*/w ratio PEG-coated NPs compared with uncoated NPs was confirmed in a second experiment where the expression of luciferase was imaged 24 h after intramuscular injection (Fig. 9A). The intramuscular injections in this experiment were performed in the gastrocnemius muscle for better imaging results. The quantified bioluminescence intensity (BLI) was significantly higher in

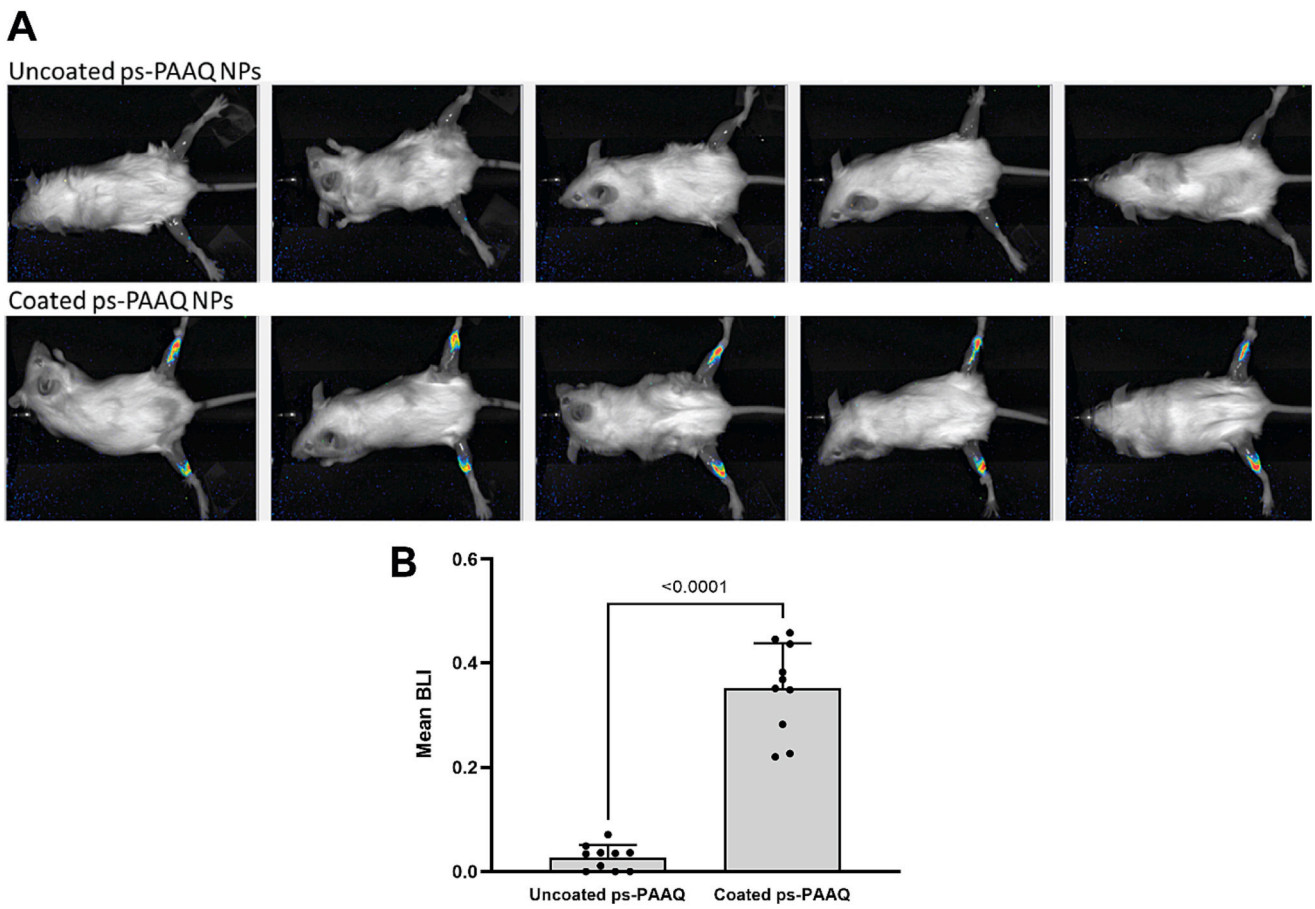

Fig. 9. Imaging of luciferase activity in mice. (A) Imaging of luciferase bioluminescence in mice 24 h after intramuscular (gastrocnemius) injection of uncoated *vs* coated ps-PAAQ NPs with luciferase mRNA. Coating of PNPs with $PGA_{7.5k}$-PEG_{5k} was done in a 1:1 *w*/w ratio. (B) Mean bioluminescence intensity (BLI) in the legs. $n = 5$ animals per group, unpaired *t*-test with Welch's correction.

the group injected with coated ps-PAAQ NPs, compared with uncoated NPs (Fig. 9B). These findings provide further evidence of the positive effect for coating ps-PAAQ NPs with $PGA_{7.5k}$-PEG_{5k} at a 1:1 *w*/w ratio.

4. Discussion

We developed a novel type of polymeric nanoparticles composed of a multi-armed ethylenediamine (Mw 800, 2 % *w*/w) that acts as a branched core to attach multiple linear poly(amidoamine) chains, possessing disulfide groups in the main chain and chloroquinoline moieties (Q) in the side chains. These positively charged nanoparticles can be efficiently loaded with mRNA and easily coated on their surface with a $PGA_{7.5k}$-PEG_{5k} block copolymer by electrostatic interaction, yielding stable nanoparticles with near neutral surface charge. The nanoparticle structure with 25 mol% Q as side groups in the ps-PAAQ polymer and a $PGA_{7.5k}$-PEG_{5k}/polymer coating ratio of 1:1 *w*/w combines excellent physicochemical properties required for application as a delivery platform, such as electroneutral surface, small size, monodisperse distribution and high stability. Moreover, this nanoparticle is more efficient in the *in vivo* reporter gene expression compared with PNPs without chloroquinoline or PEG-polymer coating.

In our *in vitro* experiments with mammalian cells, the presence of Q in the polymer resulted in remarkably higher GFP expression up to a concentration of 25 mol%. A similar enhancement was observed with luciferase activity in muscle homogenates after local delivery in mouse muscle, compared with nanoparticles without Q in the polymer. The parent molecule chloroquine (CQ), an anti-malarial drug, is a well-known endosomal escape agent [27], which has been shown to enhance gene expression by different mechanisms. The transfection enhancement by chloroquine has been attributed to several factors such as promotion of endosomal buffering, endosomal disruption, inhibition of lysosomal degradation, and electrostatic interaction with negatively charged components of the transferred genetic molecules [26,27]. The pH buffering by CQ in endocytic vesicles facilitates endosomal escape through the rupture of the endosomal membrane ("proton sponge effect") [38]. CQ also increases the effectiveness of gene delivery *via* interaction with nucleotide bases and electrostatic interaction with anionic phosphate groups of nucleic acids [39]. In our experiment with heparin competition, this interaction with nucleotide bases is supported by the observed lower mRNA release from nanoparticles containing Q in the polymer, compared with nanoparticles without Q. This stabilization against polyanions might be related to π-π stacking between the mRNA and the aromatic residues of chloroquinoline in the polymer side chains, such effect has been recently observed in micelles containing aromatic tyrosine groups [40]. Furthermore, it was previously reported that a nucleotide-binding polymer containing quinine, a quinoline derivative, significantly enhanced pDNA delivery in several human cell lines, compared with Lipofectamine 2000 [41]. Interaction between the quinoline moiety of quinine and the DNA was confirmed in this study using Raman spectroscopy.

The local administration of drug delivery systems faces many biological barriers preventing them from getting to their intended sites of action, including the skin, connective tissues and mucosal membranes [42]. Nanoparticles can penetrate a variety of tissues due to their small size and greater surface-to-volume ratio [43]. This ability, however, depends largely on their physicochemical properties. Average particle size and polydispersity index (PDI) are two of the most monitored parameters during the preclinical characterization of nanomedicines, since

they are known to impact the body absorption, biodistribution and excretion of the nanomaterials [44]. Multiple studies report the highest passive uptake and intracellular delivery when particles ~50 nm in diameter are used, regardless of the core composition or surface [45–49]. For PNPs, it is usually accepted that PDI values <0.1 represent highly monodisperse standards, whereas PDI >0.4 indicates polydisperse distribution and might affect stability of formulations [50]. In this context, our $PGA_{7.5k}$-PEG_{5k} coated ps-PAAQ nanoparticles stand out by having an average size around 50 nm in buffer solution and PDI values <0.1, which are lower compared with uncoated NPs and ideal for pharmaceutical applications.

In the particle characterization, it was clear from our results that the longer PEG_{5k} chain showed better physicochemical properties than PEG_{2k} in the PGA-PEG copolymer coating. This finding can be explained by the enhanced steric repulsion of PEG, as the distance between two NPs increases with the increase of the PEG length and more of the charges are shielded, thus preventing aggregation [51]. A longer PEG chain also increases hydrophilicity *via* an increase in ether repeats, each forming additional hydrogen bonds with the solvent [30]. These $PGA_{7.5k}$-PEG_{5k}-coated nanoparticles were also observed to be more thermally stable than uncoated nanoparticles, protecting the mRNA payload from degradation after incubation in buffer solution at 37 °C for more than a week without visible degradation. Thermally stable vaccine platforms are an urgent need for treatment of emerging infectious diseases, especially in developing regions where a continuous cold-chain logistics from the manufacturer to remote clinics is not possible [52]. Additionally, we identified an optimal coating-to-polymer weight ratio for delivery of luciferase mRNA in mice (1:1 *w*/w ratio). Compared with uncoated NPs, this ratio significantly increased the luciferase activity in muscle tissue, which might be related to the higher stability and uniform size distribution of these formulations.

Another important physical parameter for quality control of polymer-based nanoparticles is the zeta potential or surface charge. Since most cellular membranes are negatively charged, zeta potential can affect the ability of nanoparticles to permeate membranes, with cationic particles generally displaying more toxicity associated with cell wall disruption [53]. Cationic nanocarriers can induce acute cell necrosis through the interaction with Na^+/K^+-ATPase, leading to intracellular Na^+ overload [54]. The subsequent leakage of mitochondrial DNA was reported to trigger severe inflammation *in vivo*, which is mediated by a pathway involving the Toll-like receptor 9 (TLR9) and myeloid differential factor 88 (MyD88) signaling [54]. The PEGylation of nanoparticles has been shown as an efficient strategy to reduce the charge and cytotoxicity of cationic polymers [55]. In our study, the coating of cationic PNPs with $PGA_{7.5k}$-PEG_{5k} resulted in a neutral surface charge, without negatively affecting protein expression *in vitro* or *in vivo*. Visible toxic effects were not observed after IM injection of our nanoparticle formulations in mice.

Our results underline that the $PGA_{7.5k}$-PEG_{5k} copolymer integration into our delivery platform produces smaller nanoparticles, efficiently shields the surface charge, and improves thermal stability. The incorporation of Q is also advantageous as it significantly enhances transfection efficiency and improves nanoparticle stability in the presence of other polyanions. Furthermore, mRNA delivery is efficient after local administration of these nanoparticle formulations in mice, especially *via* the intramuscular route. Further investigation is needed to determine the biodistribution and exact transfected cell type *in vivo*. Mechanistic studies focusing on cell uptake and intracellular trafficking of the nanoparticles are ongoing. In addition, these bioreducible ps-PAAQ vectors are under development for application in prophylactic vaccines for infectious diseases (*e.g.*, influenza and SARS-CoV-2), therapeutic vaccines (*e.g.*, oncology) and therapeutics for chronic diseases (*e.g.*, osteoarthritis).

5. Conclusions

In this study, we demonstrated the development of improved PAA-based nanoparticles for mRNA delivery with excellent encapsulation efficiency, thermal stability and an electroneutral surface charge, all important properties for non-viral vectors in nucleotide delivery. The addition of functional Q groups to the polymer backbone and the *co*-formulation with PGA-PEG coating resulted in an improved and efficient delivery system, as shown in *in vitro* and *in vivo* experiments with different reporter genes. This promising technology is broadly applicable for the use in mRNA-based vaccines and therapeutics.

CRediT authorship contribution statement

Adriano P. Pontes: Writing – review & editing, Writing – original draft, Visualization, Methodology, Investigation, Formal analysis, Data curation, Conceptualization. **Steffen van der Wal:** Writing – review & editing, Writing – original draft, Visualization, Methodology, Investigation, Formal analysis, Data curation, Conceptualization. **Karin Roelofs:** Writing – review & editing, Visualization, Methodology, Investigation, Formal analysis, Data curation, Conceptualization. **Anne Grobbink:** Methodology, Investigation, Formal analysis, Data curation. **Laura B. Creemers:** Writing – review & editing, Validation, Supervision, Funding acquisition. **Johan F.J. Engbersen:** Writing – review & editing, Validation, Supervision, Funding acquisition, Conceptualization. **Jaap Rip:** Writing – review & editing, Validation, Supervision, Resources, Project administration, Funding acquisition, Conceptualization.

Declaration of competing interest

The authors declare the following financial interests/personal relationships which may be considered as potential competing interests: Adriano P. Pontes reports financial support was provided by Marie Sklodowska-Curie grant agreement No. 955335. Johan F.J. Engbersen reports a relationship with 20Med Therapeutics BV that includes: equity or stocks. Johan F.J. Enbersen has patent #US 9.012,424 B2 Nanogels issued to 20Med Therapeutics BV.

Data availability

Data will be made available on request.

Acknowledgements

This project has received funding from the European Union's Horizon 2020 research and innovation program under Marie Sklodowska-Curie grant agreement No. 955335.

Appendix A. Supplementary data

Supplementary data to this article can be found online at https://doi.org/10.1016/j.bioadv.2023.213713.

References

[1] A.C. Anselmo, S. Mitragotri, Nanoparticles in the clinic: an update post COVID-19 vaccines, Bioeng. Transl. Med. 6 (2021), e10246, https://doi.org/10.1002/BTM2.10246.
[2] H. Yin, R.L. Kanasty, A.A. Eltoukhy, A.J. Vegas, J.R. Dorkin, D.G. Anderson, Non-viral vectors for gene-based therapy, Nat. Rev. Genet. 15 (2014) 541–555, https://doi.org/10.1038/nrg3763.
[3] J. Conde, R. Langer, J. Rueff, mRNA therapy at the convergence of genetics and nanomedicine, Nat. Nanotechnol. 18 (2023) 537–540, https://doi.org/10.1038/s41565-023-01347-w.
[4] R. Tenchov, R. Bird, A.E. Curtze, Q. Zhou, Lipid nanoparticles from liposomes to mRNA vaccine delivery, a landscape of research diversity and advancement, ACS Nano 15 (2021) 16982–17015, https://doi.org/10.1021/acsnano.1c04996.

[5] W. Yang, L. Mixich, E. Boonstra, H. Cabral, Polymer-based mRNA delivery strategies for advanced therapies, Adv. Healthc. Mater. 12 (2023) 2202688, https://doi.org/10.1002/adhm.202202688.

[6] C.-K. Chen, P.-K. Huang, W.-C. Law, C.-H. Chu, N.-T. Chen, L.-W. Lo, Biodegradable polymers for gene-delivery applications, Int. J. Nanomedicine 15 (2020) 2131–2150, https://doi.org/10.2147/IJN.S222419.

[7] P. Patel, N.M. Ibrahim, K. Cheng, The importance of apparent pKa in the development of nanoparticles encapsulating siRNA and mRNA, Trends Pharmacol. Sci. 42 (2021) 448–460, https://doi.org/10.1016/j.tips.2021.03.002.

[8] O. Boussif, F. Lezoualc'h, M.A. Zanta, M.D. Mergny, D. Scherman, B. Demeneix, J. P. Behr, A versatile vector for gene and oligonucleotide transfer into cells in culture and in vivo: polyethylenimine, Proc. Natl. Acad. Sci. U. S. A. 92 (1995) 7297–7301, https://doi.org/10.1073/PNAS.92.16.7297.

[9] P. Ferruti, E. Ranucci, New functional polymers for medical applications, Polym. J. 23 (1991) 541–550, https://doi.org/10.1295/polymj.23.541.

[10] C. Lin, Z. Zhong, M.C. Lok, X. Jiang, W.E. Hennink, J. Feijen, J.F.J. Engbersen, Linear poly(amido amine)s with secondary and tertiary amino groups and variable amounts of disulfide linkages: synthesis and in vitro gene transfer properties, J. Control. Release 116 (2006) 130–137, https://doi.org/10.1016/J.JCONREL.2006.09.009.

[11] J.J. Green, J. Shi, E. Chiu, E.S. Leshchiner, R. Langer, D.G. Anderson, Biodegradable polymeric vectors for gene delivery to human endothelial cells, Bioconjug. Chem. 17 (2006) 1162–1169, https://doi.org/10.1021/BC0600968.

[12] H. Guerrero-Cázares, S.Y. Tzeng, N.P. Young, A.O. Abutaleb, A. Quiñones-Hinojosa, J.J. Green, Biodegradable polymeric nanoparticles show high efficacy and specificity at DNA delivery to human glioblastoma in vitro and in vivo, ACS Nano 8 (2014) 5141–5153, https://doi.org/10.1021/nn501197v.

[13] Y. Sun, L. Xian, J. Yu, T. Yang, J. Zhang, Z. Yang, J. Jiang, C. Cai, X. Zhao, L. Yang, P. Ding, Structure–function correlations of poly(amido amine)s for gene delivery, Macromol. Biosci. 17 (2017) 1600297, https://doi.org/10.1002/MABI.201600297.

[14] J. Zhang, X. Cai, R. Dou, C. Guo, J. Tang, Y. Hu, H. Chen, J. Chen, Poly(β-amino ester)s-based nanovehicles: structural regulation and gene delivery, Mol. Ther. Nucleic Acids 32 (2023) 568–581, https://doi.org/10.1016/j.omtn.2023.04.019.

[15] C. Lin, Z. Zhong, M.C. Lok, X. Jiang, W.E. Hennink, J. Feijen, J.F.J. Engbersen, Novel bioreducible poly(amido amine)s for highly efficient gene delivery, Bioconjug. Chem. 18 (2007) 138–145, https://doi.org/10.1021/bc060200l.

[16] C. Lin, C.-J. Blaauboer, M.M. Timoneda, M.C. Lok, M. Steenbergen, W.E. Hennink, Z. Zhong, J. Feijen, J.F.J. Engbersen, Bioreducible poly(amido amine)s with oligoamine side chains: synthesis, characterization, and structural effects on gene delivery, J. Control. Release 126 (2008) 166–174, https://doi.org/10.1016/j.jconrel.2007.11.012.

[17] C. Lin, J.F.J. Engbersen, Effect of chemical functionalities in poly(amido amine)s for non-viral gene transfection, J. Control. Release 132 (2008) 267–272, https://doi.org/10.1016/j.jconrel.2008.06.022.

[18] C. Lin, J.F.J. Engbersen, PEGylated bioreducible poly(amido amine)s for non-viral gene delivery, Mater. Sci. Eng. C 31 (2011) 1330–1337, https://doi.org/10.1016/j.msec.2011.04.017.

[19] L.J. van der Aa, P. Vader, G. Storm, R.M. Schiffelers, J.F.J. Engbersen, Optimization of poly(amido amine)s as vectors for siRNA delivery, J. Control. Release 150 (2011) 177–186, https://doi.org/10.1016/j.jconrel.2010.11.030.

[20] A.K. Blakney, Y. Zhu, P.F. McKay, C.R. Bouton, J. Yeow, J. Tang, K. Hu, K. Samnuan, C.L. Grigsby, R.J. Shattock, M.M. Stevens, Big is beautiful: enhanced saRNA delivery and immunogenicity by a higher molecular weight, bioreducible, cationic polymer, ACS Nano 14 (2020) 5711–5727, https://doi.org/10.1021/ACSNANO.0C00326.

[21] M. Piest, C. Lin, M.A. Mateos-Timoneda, M.C. Lok, W.E. Hennink, J. Feijen, J.F. J. Engbersen, Novel poly(amido amine)s with bioreducible disulfide linkages in their diamino-units: structure effects and in vitro gene transfer properties, J. Control. Release 130 (2008) 38–45, https://doi.org/10.1016/j.jconrel.2008.05.023.

[22] F. Martello, M. Piest, J.F.J. Engbersen, P. Ferruti, Effects of branched or linear architecture of bioreducible poly(amido amine)s on their in vitro gene delivery properties, J. Control. Release 164 (2012) 372–379, https://doi.org/10.1016/j.jconrel.2012.07.029.

[23] M.R. Elzes, N. Akeroyd, J.F.J. Engbersen, J.M.J. Paulusse, Disulfide-functional poly (amido amine)s with tunable degradability for gene delivery, J. Control. Release 244 (2016) 357–365, https://doi.org/10.1016/j.jconrel.2016.08.021.

[24] H.J. Forman, H. Zhang, A. Rinna, Glutathione: overview of its protective roles, measurement, and biosynthesis, Mol. Aspects Med. 30 (2009) 1–12, https://doi.org/10.1016/J.MAM.2008.08.006.

[25] L.M.P. Vermeulen, T. Brans, S.K. Samal, P. Dubruel, J. Demeester, S.C. De Smedt, K. Remaut, K. Braeckmans, Endosomal size and membrane leakiness influence proton sponge-based rupture of endosomal vesicles, ACS Nano 12 (2018) 2332–2345, https://doi.org/10.1021/acsnano.7b07583.

[26] D. Pei, M. Buyanova, Overcoming endosomal entrapment in drug delivery, Bioconjug. Chem. 30 (2019) 273–283, https://doi.org/10.1021/acs.bioconjchem.8b00778.

[27] M. Hajimolaali, H. Mohammadian, A. Torabi, A. Shirini, M. Khalife Shal, H. Barazandeh Nezhad, S. Iranpour, R. Baradaran Eftekhari, F. Dorkoosh, Application of chloroquine as an endosomal escape enhancing agent: new frontiers for an old drug, Expert Opin. Drug Deliv. 18 (2021) 877–889, https://doi.org/10.1080/17425247.2021.1873272.

[28] K.B. Knudsen, H. Northeved, E.K. Pramod Kumar, A. Permin, T. Gjetting, T. L. Andresen, S. Larsen, K.M. Wegener, J. Lykkesfeldt, K. Jantzen, S. Loft, P. Møller, M. Roursgaard, In vivo toxicity of cationic micelles and liposomes, Nanomed. Nanotechnol. Biol. Med. 11 (2015) 467–477, https://doi.org/10.1016/J.NANO.2014.08.004.

[29] A. Sukhanova, S. Bozrova, P. Sokolov, M. Berestovoy, A. Karaulov, I. Nabiev, Dependence of nanoparticle toxicity on their physical and chemical properties, Nanoscale Res. Lett. 13 (2018) 44, https://doi.org/10.1186/S11671-018-2457-X.

[30] J.V. Jokerst, T. Lobovkina, R.N. Zare, S.S. Gambhir, Nanoparticle PEGylation for imaging and therapy, Nanomed 6 (2011) 715–728, https://doi.org/10.2217/nnm.11.19.

[31] A.A. D'souza, R. Shegokar, Polyethylene glycol (PEG): a versatile polymer for pharmaceutical applications, Expert Opin. Drug Deliv. 13 (2016) 1257–1275, https://doi.org/10.1080/17425247.2016.1182485.

[32] L. Shi, J. Zhang, M. Zhao, S. Tang, X. Cheng, W. Zhang, W. Li, X. Liu, H. Peng, Q. Wang, Effects of polyethylene glycol on the surface of nanoparticles for targeted drug delivery, Nanoscale 13 (2021) 10748–10764, https://doi.org/10.1039/D1NR02065J.

[33] D.E. Owens, N.A. Peppas, Opsonization, biodistribution, and pharmacokinetics of polymeric nanoparticles, Int. J. Pharm. 307 (2006) 93–102, https://doi.org/10.1016/j.ijpharm.2005.10.010.

[34] S.M. Moghimi, D. Simberg, E. Papini, Z.S. Farhangrazi, Complement activation by drug carriers and particulate pharmaceuticals: principles, challenges and opportunities, Adv. Drug Deliv. Rev. 157 (2020) 83–95, https://doi.org/10.1016/j.addr.2020.04.012.

[35] X. Hou, T. Zaks, R. Langer, Y. Dong, Lipid nanoparticles for mRNA delivery, Nat. Rev. Mater. 6 (2021) 1078–1094, https://doi.org/10.1038/s41578-021-00358-0.

[36] J.K. Natarajan, J.N. Alumasa, K. Yearick, K.A. Ekoue-Kovi, L.B. Casabianca, A.C. De Dios, C. Wolf, P.D. Roepe, 4-N-, 4-S-, and 4-O-chloroquine analogues: influence of side chain length and quinolyl nitrogen pKa on activity vs chloroquine resistant malaria, J. Med. Chem. 51 (2008) 3466–3479, https://doi.org/10.1021/jm701478a.

[37] A. Zintchenko, L.J. Van Der Aa, J.F.J. Engbersen, Improved synthesis strategy of poly(amidoamine)s for biomedical applications: catalysis by "green" biocompatible earth alkaline metal salts, Macromol. Rapid Commun. 32 (2011) 321–325, https://doi.org/10.1002/MARC.201000545.

[38] E.C. Freeman, L.M. Weiland, W.S. Meng, Modeling the proton sponge hypothesis: examining proton sponge effectiveness for enhancing intracellular gene delivery through multiscale modelling, J. Biomater. Sci. Polym. Ed. 24 (2013) 398–416, https://doi.org/10.1080/09205063.2012.690282.

[39] J. Cheng, R. Zeidan, S. Mishra, A. Liu, S.H. Pun, R.P. Kulkarni, G.S. Jensen, N. C. Bellocq, M.E. Davis, Structure-function correlation of chloroquine and analogues as transgene expression enhancers in nonviral gene delivery, J. Med. Chem. 49 (2006) 6522–6531, https://doi.org/10.1021/jm060736s.

[40] W. Yang, T. Miyazaki, Y. Nakagawa, E. Boonstra, K. Masuda, Y. Nakashima, P. Chen, L. Mixich, K. Barthelmes, A. Matsumoto, P. Mi, S. Uchida, H. Cabral, Block catiomers with flanking hydrolyzable tyrosinate groups enhance in vivo mRNA delivery via π–π stacking-assisted micellar assembly, Sci. Technol. Adv. Mater. 24 (2023) 2170164, https://doi.org/10.1080/14686996.2023.2170164.

[41] C. Van Bruggen, D. Punihaole, A.R. Keith, A.J. Schmitz, J. Tolar, R.R. Frontiera, T. M. Reineke, Quinine copolymer reporters promote efficient intracellular DNA delivery and illuminate a protein-induced unpackaging mechanism, PNAS 117 (2020) 32919–32928, https://doi.org/10.1073/pnas.2016860117.

[42] T. Ji, D.S. Kohane, Nanoscale systems for local drug delivery, Nano Today 28 (2019), 100765, https://doi.org/10.1016/j.nantod.2019.100765.

[43] L. Yildirimer, N.T.K. Thanh, M. Loizidou, A.M. Seifalian, Toxicological considerations of clinically applicable nanoparticles, Nano Today 6 (2011) 585–607, https://doi.org/10.1016/j.nantod.2011.10.001.

[44] S. Gioria, F. Caputo, P. Urbán, C.M. Maguire, S. Bremer-Hoffmann, A. Prina-Mello, L. Calzolai, D. Mehn, Are existing standard methods suitable for the evaluation of nanomedicines: some case studies, Nanomed 13 (2018) 539–554, https://doi.org/10.2217/nnm-2017-0338.

[45] W. Jiang, B.Y.S. Kim, J.T. Rutka, W.C.W. Chan, Nanoparticle-mediated cellular response is size-dependent, Nat. Nanotechnol. 3 (2008) 145–150, https://doi.org/10.1038/nnano.2008.30.

[46] F. Lu, S.H. Wu, Y. Hung, C.Y. Mou, Size effect on cell uptake in well-suspended, uniform mesoporous silica nanoparticles, Small 5 (2009) 1408–1413, https://doi.org/10.1002/SMLL.200900005.

[47] L.Q. Chen, L. Fang, J. Ling, C.Z. Ding, B. Kang, C.Z. Huang, Nanotoxicity of silver nanoparticles to red blood cells: size dependent adsorption, uptake, and hemolytic activity, Chem. Res. Toxicol. 28 (2015) 501–509, https://doi.org/10.1021/TX500479M.

[48] M. Danaei, M. Dehghankhold, S. Ataei, F.H. Davarani, R. Javanmard, A. Dokhani, S. Khorasani, M.R. Mozafari, Impact of particle size and polydispersity index on the clinical applications of lipidic nanocarrier systems, Pharmaceutics 10 (2018) 57, https://doi.org/10.3390/pharmaceutics10020057.

[49] M.J. Mitchell, M.M. Billingsley, R.M. Haley, M.E. Wechsler, N.A. Peppas, R. Langer, Engineering precision nanoparticles for drug delivery, Nat. Rev. Drug Discov. 20 (2020) 101–124, https://doi.org/10.1038/s41573-020-0090-8.

[50] Y. Takechi-Haraya, T. Ohgita, Y. Demizu, H. Saito, K.-I. Izutsu, K. Sakai-Kato, Current status and challenges of analytical methods for evaluation of size and surface modification of nanoparticle-based drug formulations, AAPS PharmSciTech 23 (2022) 150, https://doi.org/10.1208/s12249-022-02303-y.

[51] Y. Jiang, T.P. Lodge, T.M. Reineke, Packaging pDNA by polymeric ABC micelles simultaneously achieves colloidal stability and structural control, J. Am. Chem. Soc. 140 (2018) 11101–11111, https://doi.org/10.1021/JACS.8B06309.

[52] R. Kumar, V. Srivastava, P. Baindara, A. Ahmad, Thermostable vaccines: an innovative concept in vaccine development, Expert Rev. Vaccines 21 (2022) 811–824, https://doi.org/10.1080/14760584.2022.2053678.

[53] J.D. Clogston, A.K. Patri, Zeta potential measurement, in: S.E. McNeil (Ed.), Characterization of Nanoparticles Intended for Drug Delivery, Methods Mol. Biol., 697, 2011, pp. 63–70, https://doi.org/10.1007/978-1-60327-198-1_6.
[54] X. Wei, B. Shao, Z. He, T. Ye, M. Luo, Y. Sang, X. Liang, W. Wang, S. Luo, S. Yang, S. Zhang, C. Gong, M. Gou, H. Deng, Y. Zhao, H. Yang, S. Deng, C. Zhao, L. Yang, Z. Qian, J. Li, X. Sun, J. Han, C. Jiang, M. Wu, Z. Zhang, Cationic nanocarriers induce cell necrosis through impairment of Na+/K+-ATPase and cause subsequent inflammatory response, Cell Res. 25 (2015) 237–253, https://doi.org/10.1038/cr.2015.9.
[55] J.S. Suk, Q. Xu, N. Kim, J. Hanes, L.M. Ensign, PEGylation as a strategy for improving nanoparticle-based drug and gene delivery, Adv. Drug Deliv. Rev. 99 (2016) 28–51, https://doi.org/10.1016/j.addr.2015.09.012.